Journal of Environmental Management 336 (2023) 117693

Contents lists available at ScienceDirect

Journal of Environmental Management

journal homepage: www.elsevier.com/locate/jenvman

Research article

From UAV to PlanetScope: Upscaling fractional cover of an invasive species *Rosa rugosa*

Thaísa F. Bergamo [a,b,*,1], Raul Sampaio de Lima [a,1], Tiiu Kull [a], Raymond D. Ward [c,a], Kalev Sepp [a], Miguel Villoslada [b,a]

[a] Institute of Agriculture and Environmental Sciences, Estonian University of Life Sciences, Kreutzwaldi 5, EE-51006, Tartu, Estonia
[b] Department of Geographical and Historical Studies, University of Eastern Finland, P.O. Box 111, FI-80101, Joensuu, Finland
[c] Centre for Aquatic Environments, School of the Environment and Technology, University of Brighton, Cockcroft Building, Moulsecoomb, Brighton, BN2 4GJ, UK

ARTICLE INFO

Keywords:
Unoccupied aerial vehicles
Coast
Invasive species
Satellite
Machine learning
Rosa rugosa
Estonia
Baltic

ABSTRACT

Invasive plant species pose a direct threat to biodiversity and ecosystem services. Among these, *Rosa rugosa* has had a severe impact on Baltic coastal ecosystems in recent decades. Accurate mapping and monitoring tools are essential to quantify the location and spatial extent of invasive plant species to support eradication programs. In this paper we combined RGB images obtained using an Unoccupied Aerial Vehicle, with multispectral PlanetScope images to map the extent of *R. rugosa* at seven locations along the Estonian coastline. We used RGB-based vegetation indices and 3D canopy metrics in combination with a random forest algorithm to map *R. rugosa* thickets, obtaining high mapping accuracies (Sensitivity = 0.92, specificity = 0.96). We then used the *R. rugosa* presence/absence maps as a training dataset to predict the fractional cover based on multispectral vegetation indices derived from the PlanetScope constellation and an Extreme Gradient Boosting algorithm (XGBoost). The XGBoost algorithm yielded high fractional cover prediction accuracies (RMSE = 0.11, R^2 = 0.70). An in-depth accuracy assessment based on site-specific validations revealed notable differences in accuracy between study sites (highest R^2 = 0.74, lowest R^2 = 0.03). We attribute these differences to the various stages of *R. rugosa* invasion and the density of thickets. In conclusion, the combination of RGB UAV images and multispectral PlanetScope images is a cost-effective method to map *R. rugosa* in highly heterogeneous coastal ecosystems. We propose this approach as a valuable tool to extend the highly local geographical scope of UAV assessments into wider areas and regional evaluations.

1. Introduction

Invasive plant species have a direct impact on ecosystem structure and function worldwide (Weidlich et al., 2020), affecting biodiversity and the supply of ecosystem services. The fast pace and aggressivity of invasions can also cause severe economic losses (Haubrock et al., 2021) and compromise iconic landscapes of very high cultural value (Junk & da Cunha, 2012). Invasive plant species can also modify soil and other physical conditions in ways that increase their own fitness relative to that of native species (Jordan et al., 2008).

Coastal ecosystems are particularly susceptible to invasive species, due to the occurrence of sensitive habitats (e.g. sand dunes, coastal meadows, seagrass meadows, and coral reefs) and protected and rare species (Carboni et al., 2010; Pardini et al., 2015). One of the most troublesome invasive plant species in natural or semi-natural habitats of northern Europe is *Rosa rugosa* (Kelager et al., 2013). This species native range spreads throughout China, the Korean peninsula, Japan and the Kamchatka peninsula (Zhang et al., 2018). *R. rugosa* was introduced to Europe as an ornamental and sand dune fixing plant in the 19th Century (Menkis et al., 2014). In coastal areas of the Baltic Sea, *R. rugosa* constitutes a major coastal ecosystem invasive, predominantly in sand dunes and coastal meadows (Kunttu and Kunttu, 2019). The first naturalized record of *R. rugosa* in Europe was in Germany in 1845 (Zhang et al., 2018). This invasive shrub strongly outcompetes other species in sand dunes and coastal meadows, ultimately turning these habitats into dense, monospecific *R. rugosa* thickets (Bruun, 2006). On sand dunes *R. rugosa* increases soil organic carbon, total nitrogen and phosphate, which hinders the recovery of the habitat even after the removal of the

* Corresponding author. Institute of Agriculture and Environmental Sciences, Estonian University of Life Sciences, Kreutzwaldi 5, EE-51006, Tartu, Estonia.
E-mail address: thaisafbergamo@gmail.com (T.F. Bergamo).
[1] Thaísa F. Bergamo and Raul Sampaio de Lima contributed equally to this work. First co-authors are listed in alphabetical order.

https://doi.org/10.1016/j.jenvman.2023.117693
Received 17 January 2023; Received in revised form 28 February 2023; Accepted 6 March 2023
Available online 11 March 2023

species (Stefanowicz et al., 2019). In addition to the threat to biodiversity and ecosystem services in coastal areas of the Baltic Sea, control and eradication measures are costly and labour-intensive. In coastal areas, the common challenges associated with satellite-based remote sensing, such as coarse ground sampling distance (GSD) and sub-pixel spectral mixing, are amplified by the geomorphological structure of coastlines. Highly sensitive ecosystems such as sandy beaches, including dune areas, occur as very narrow bands along the coast, often just a few meters wide. This, in combination with the spectral nature of seawater, renders the use of medium resolution satellite missions (e.g. Sentinel 2 and Landsat missions) challenging for invasive species mapping.

For decades, monitoring of invasion processes has relied on plot-based sampling and monitoring (Cheney et al., 2018; Pickart et al., 1998). However, the local and spatially-constrained nature of these methods hinders our ability to fully understand the dynamics and spatial nature of invasions. Moreover, plot-based assessments can only provide a rough approximation of the extent of the areas affected, consequently compromising eradication efforts undertaken by public agencies and practitioners.

Shifting towards accurate continuous cover data to map the extent and spread dynamics of invasive plant species has become a priority in conservation science, policy and practice (Caplat et al., 2012; Lehmann et al., 2017). The wide range of remote sensing instruments and platforms available nowadays constitute an ideal toolset to overcome the limitations associated with traditional monitoring methods. The multiple spatial, spectral, and temporal resolutions associated with past and present satellite missions allow for accurate spatial representations of plant species invasions (Kattenborn et al., 2019; Martin et al., 2018). In addition, the latest advances in machine and deep learning techniques have reduced the computational challenges involved in the processing of very large datasets (Díaz-Ramírez, 2021), the classification of spectrally-similar vegetation types (Beyer et al., 2019), or modelling complex ecosystem structures and functions (Dong et al., 2021). Many studies have taken advantage of the combination of satellite and airborne remote sensing data and artificial intelligence to map and monitor invasive plant species. Kattenborn et al. (2019) used Unoccupied Aerial Vehicle (UAV)-based reference data and random forest models with multitemporal Sentinel −1 and −2 data to predict the canopy cover of woody invasive species. In another work, the fractional cover of the invasive shrub species *Ulex europaeus* was estimated based on high-resolution UAV images and a medium resolution intra-annual time-series of Sentinel-2 (Gränzig et al., 2021).

In this study, we use the term Unoccupied Aerial Vehicles, as encouraged by Joyce et al. (2021). Unoccupied Aerial Vehicles (UAVs), have the capacity to evaluate the fine spatial scale of ecosystem structures, functions and processes that may be "invisible" to medium resolution satellite sensors. Moreover, the flexibility of deployment and ability to carry various sensors (e.g. red green blue [RGB], multispectral, LiDAR, or thermal), boost the potential of UAVs to map invasive plant species. Not surprisingly, several studies have tested UAV-based approaches for detecting and mapping invasive plant species (Papp et al., 2021). However, UAVs are strongly limited by relatively short flight time capabilities, and the large size of the datasets generated. This, in turn, limits the capacity of UAV to provide consistent data over large spatial extents.

In recent years, a range of high and very high spatial resolution satellite missions have emerged, revolutionizing the fields of remote sensing and biodiversity monitoring. More specifically, Planet Labs Inc. Operates a constellation of over 180 CubeSats that supply multispectral imagery in ground sampling distances (GSD) under 4.1 m per pixel (Roy et al., 2021). The PlanetScope constellation has proven useful for various applications such as detection of forest change (Francini et al., 2020), monitoring pasture aboveground biomass (Dos Reis et al., 2020) and detection and mapping of invasive plant species (Theron et al., 2022; Lake et al., 2022). Several works have also demonstrated the benefits of combining PlanetScope and UAV data, providing improved estimations of above-ground biomass (Mao et al., 2022), occurrence of invasive plant species (Marzialetti et al., 2022), and estimations of leaf phenology (Wu et al., 2021).

Regarding methodological approaches, two main image classification techniques have been employed for invasive species detection and mapping: pixel-based and object-based (Hussain et al., 2013). Pixel-based approaches have traditionally been used for classification, and one of the benefits to this, is the capacity to detect small patches of plant species or even isolated individuals (Ouyang et al., 2011), allowing early mitigation strategies for managing invasive species to be put in place. However, the efficiency of these strategies is constrained by spectrally complex and mixed information (Hussain et al., 2013). However, object-based approaches, perform spectrally homogeneous area or object segmentation, integrating textural, shape, and contextual information in the classification framework (Mafanya et al., 2017), and this method works well with complex datasets. It has been shown that these strategies are effective in differentiating herbaceous plant species (Ouyang et al., 2011). Despite this, several studies have shown that when applied to very high-resolution data, pixel-based approaches still outperform object-based methods (e.g., Mafanya et al., 2017; Sampedro and Mena, 2018), illustrating their suitability for accurate mapping of invasive plant species using these types of data. Within the pixel-based classification realm, both machine and deep learning algorithms have been widely used for the identification and mapping of invasive plant species. Shiferaw et al. (2019) explored the performance of five machine learning algorithms for mapping the fractional cover of *Prosopis juliflora* in a dryland ecosystem, highlighting the high accuracies obtained with a random forest regressor. Within the domain of deep learning, James and Bradshaw (2020) used the U-NET architecture to accurately map shrubs of the *Hakea* genus.

Despite the wide range of invasive species addressed in the literature, and methods and sensors utilized, currently there is limited knowledge on the feasibility of combining UAV RGB images and satellite scenes to monitor *R. rugosa* invasions. In addition, very few studies have analyzed the ability of machine learning algorithms to predict the occurrence of invasive species beyond the geographical scope of training datasets. In this study, we aim at tackling the challenges associated with mapping the occurrence and extent of *Rosa rugosa* in coastal areas, developing a methodology based on the combination of UAV RGB data and very high-resolution multispectral satellite data derived from the PlanetScope constellation. Specifically, we used red, green and blue UAV images to derive a set of vegetation indices and 3D canopy metrics. We then used these to map *R. rugosa* along the Estonian coast and train a *R. rugosa* fractional cover model based on PlanetScope imagery. Finally, we tested model accuracies based on site-by-site and external validation approaches.

2. Materials and methods

2.1. Study sites

Estonia's long and intricate coastline (3794 km) includes a diverse mosaic of bays, peninsulas, islands, islets and coastal wetlands (Villoslada et al., 2021). Among the various habitats occurring along the Estonian coast, sand dunes, Boreal Baltic sandy beaches, and Boreal Baltic Coastal Meadows are highly biodiverse and host a range of rare and protected vascular plant species, such as *Eryngium maritimum*, *Lathyrus japonicus* var. *Maritimus*, and *Pulsatilla pratensis*. We selected seven study sites (Fig. 1), where thickets of *R. rugosa* occur along the coast. We selected the study sites following a gradient of protection status, from National Park to areas without protection. An in-detail description of the study sites is provided in Table S1 (supplementary materials).

R. rugosa is highly invasive in Estonia and its occurrence was first mentioned in Tartu Botanical Garden in 1825 (Kukk, 1999). In 1950s there were only two regions where it had spread but nowadays it occurs

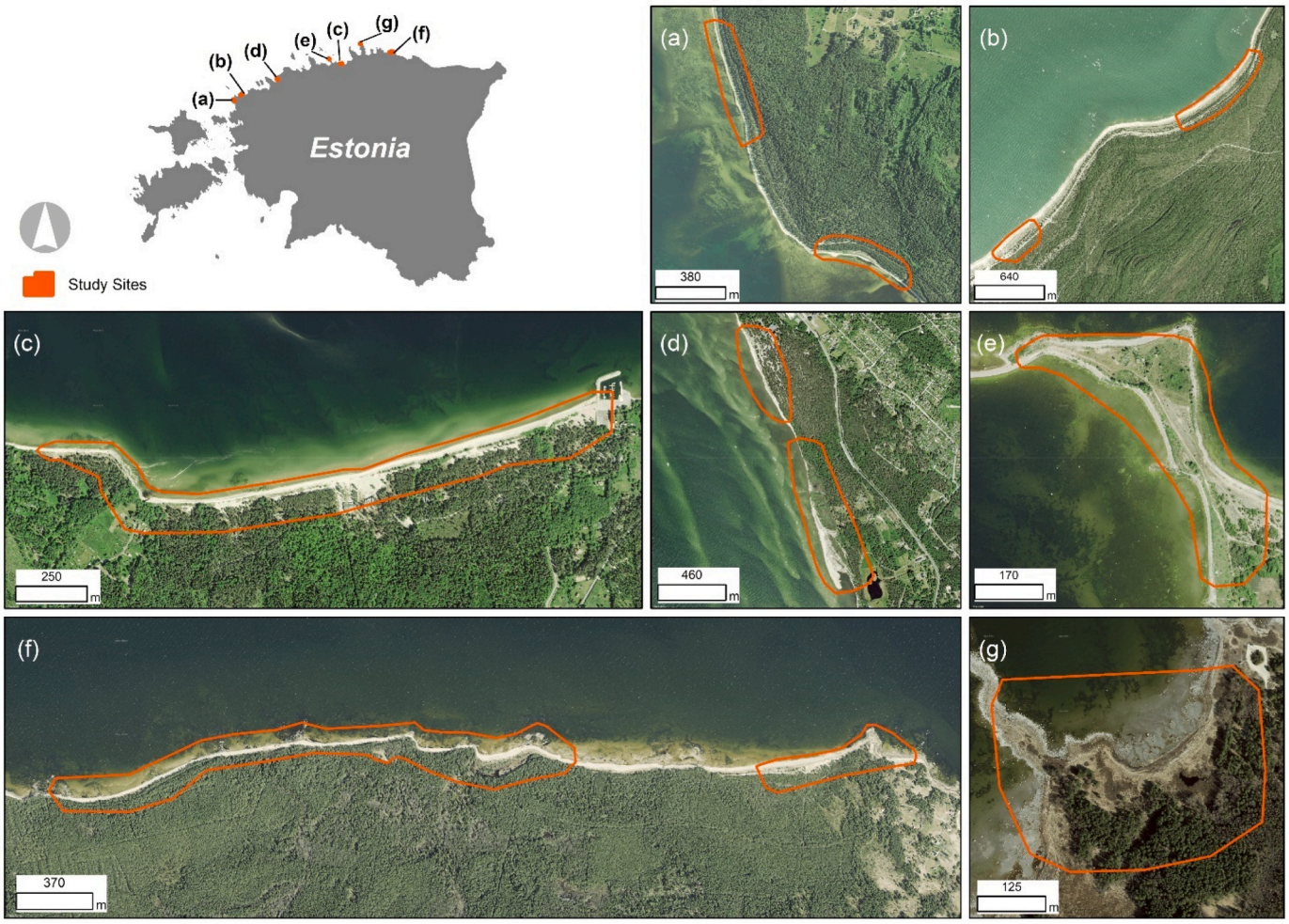

Fig. 1. Location of study sites along the Estonian coastline. (a) Rooslepa (b) Nõva, (c) Valkla, (d) Laulasmaa, (e) Neeme, (f) Vainupea, (g) Pärispea.

on most sandy beaches. It has been grown in gardens and planted on road sides, therefore it is widely spread in many inland sites.

2.2. Acquisition of UAV images, satellite images and pre-processing

We undertook 21 UAV surveys in seven study sites (Fig. 1) using a multirotor DJI Phantom 4 RTK, between July 2021 and June 2022. The UAV was equipped with an on-board Global Network Satellite System Real-Time Kinematics (GNSS-RTK) receiver, which allows for positional XYZ-accuracy of ca. 1.5 cm (Nota et al., 2022). All flights were conducted following double-grid pathways at 109 m above ground level, which yielded a ground sampling distance (GSD) of approximately 3 cm/pixel. Overlaps were set to 80%, with a gimbal angle of −80° (i.e., oblique flights), and white balance compensation set according to the illumination conditions. Moreover, the inclination of the flight grids had minor on-site adjustments from the north-south direction in order to maximize the batteries' endurance. The UAV was equipped with a DJI FC6310R camera with a 20-megapixel, 1" sensor size, and 8.8 mm focal length. The purpose of these flights was to produce othomosaics corresponding to the red, green, and blue bands and to generate a set of photogrammetric point clouds and derive canopy metrics.

We imported the resulting images in Pix4D v.4.3.31®, where the RGB orthomosaics and 3D point clouds were built. For this, we selected a full tie-point image scale for initial processing, an optimal point density, a minimum of three tie-points per processed image, and point densification based on half of the image scale (Vafidis et al., 2021).

Within the same workflow, we created photogrammetric 3D point clouds at each study site using the Structure-from Motion (SfM) in combination with the Multi-View stereo photogrammetry algorithm (SfM-MVS) (Smith et al., 2016), both implemented in Pix4D v.4.3.31®. As described by Westoby et al. (2012), the SfM generates 3D point clouds from sets of photographs through a three-step process. Firstly, a set of common keypoints is detected across the set of images using a Scale Invariant Feature Transform (SIFT). Subsequently, camera locations and orientations are used to extract a low-density 3D point cloud. Finally, the 3D point clouds are densified and transformed from a relative into an absolute 3D coordinate system. This provided an average of 92.4% of images enabled for processing, a re-projection error of 0.17 pixels, and a point density of 74.5 points per square meter. Thus, we obtained a total of 21 orthomosaics (one mosaic per band per survey) and 3D point clouds (one per survey).

We obtained the satellite images from the PlanetScope satellite constellation. PlanetScope satellites are equipped with a four-band frame imager with a split-frame NIR filter, acquiring images with an orthorectified pixel size of 3.125 m in the blue (455–515 nm), green (500–590 nm), red (59–670 nm), and near infrared (780–860 nm) wavelengths. These products were previously corrected to bottom-of-atmosphere reflectance using the 6SV2.1 radiative transfer algorithm, which accounts for a range of atmospheric, surface, and spectral conditions, and applies them to standard atmospheric models with MODIS water vapour, ozone, and aerosol data (Frazier and Hemingway, 2021). We selected one scene of PlanetScope satellite for each location, refining the scene search for 15 days around the date of UAV flight missions, less than 10% cloud cover, and complete coverage of study areas.

2.3. Predictor variables: Vegetation indices and 3D canopy metrics

A wide array of visible spectral vegetation indices have been developed in recent years, primarily based on the notion that healthy vegetation reflects a larger amount of light in the green bands compared to red and blue in the RGB normalized colour space (Yang et al., 2015; Marcial-Pablo et al., 2019). Although less robust than multispectral indices, RGB indices allow for the use of less costly field equipment, while showing adequate vegetation types and vegetation status discerning capabilities (Anderson et al., 2016; De Swaef et al., 2021).

In this study we selected 10 vegetation indices commonly used in the scientific literature (Table S2, supplementary materials). Before computing the indices in R v.4.1.3, we subjected the individual bands to a two-step normalization process, as described in Marcial-Pablo et al. (2019) and Guijarro et al. (2011).

I) Each individual band is normalized to a 0 to 1 scale using the following equations:

$$R_n = \frac{R}{R_{max}} \quad G_n = \frac{G}{G_{max}} \quad B_n = \frac{B}{B_{max}}$$

where R_n, G_n and B_n are the rescaled values of each band, and R_{max}, G_{max} and B_{max} are the maximum band values in the o to 255 scale.

II) Each individual band is normalized in the RGB colour space:

$$r = \frac{R_n}{R_n + G_n + B_n} \quad g = \frac{G_n}{R_n + G_n + B_n} \quad b = \frac{B_n}{R_n + G_n + B_n}$$

In addition to the VIs, we computed the dissimilarity index based on the grey-level co-occurrence matrix (GLCM). GLCM dissimilarity estimates the grey level distance between pairs of pixels and quantifies similarities and dissimilarities between pairs of pixels (Park and Guldmann, 2020). We calculated the GLCM dissimilarity for each study site based on the UAV-derived RGB images in the *glcm* package (Zvoleff, 2020) in R Studio.

In an effort to better capture vegetation structure and discern vegetation classes (Hantson et al., 2012; da Silva et al., 2022; de Lima et al., 2022), we also computed nine canopy metrics based on the 3D point clouds. Before performing the computations, noise points were filtered with statistical outlier removal (SOR) filters, while a cloth simulation filtering (CSF) algorithm classified ground points. These operations were implemented using the functions *classify_noise* and *classify_ground* in the lidR package (Roussel et al., 2020) in R. The SOR filter evaluates statistical parameters in the proximity of each point in the point cloud and removes those that lie beyond the set of points' standard range (i.e., standard deviation of the mean). Within the SOR filter, we set the number of neighbours to the 50 nearest points and applied one standard deviation to exclude outliers. The CSF algorithm inverts the point cloud along the z-axis, fits a surface to the inverted cloud, and classifies each point as ground or off-ground based on a distance threshold. For this procedure, we applied the "Flat terrain" option, enabled slope processing, and the classification threshold to 0.1 (Klápště et al., 2020). We adjusted the cloth resolution to 3 m, since it retrieved the best separation between ground point and low vegetation for our datasets. Using these methods, points were subsequently classified either as "ground" or as "non-ground". For normalization, the terrain elevation was estimated using a Triangulated Irregular Network (TIN) algorithm to avoid excessive occlusions in the Digital Terrain Model (DTM) (Ward et al., 2013; Neuville et al., 2021). For the Canopy Height Models (CHM), empty cells were filled using the RSAGA's function "Close Gaps", which uses the surrounding values for the interpolation (Kemper et al., 2022).

From the normalized point clouds, we calculated the density of points, maximum height, mean height, skewness of height distribution, and kurtosis of height distribution using the lidR package in R. We used the RSAGA package (Brenning et al., 2018) to calculate the Slope, Convergence Index (CI), Terrain Ruggedness Index (TRI), and Plane Curvature (CPLAN) to provide 3D spatial information for describing distinct surface features (e.g., bare soil, water, and vegetation types) (Drăguţ and Blaschke, 2006; Lee et al., 2020). The skewness and kurtosis measure the amount of information deviating from the normal distribution (Zhao et al., 2018). The skewness describes the degree of symmetry of the distribution, while the kurtosis describes the shape and magnitude of the distribution tails. The slope represents the highest rate of change in the elevation to the adjacent pixel (Dornik et al., 2018). Plane Curvature describes the variation of aspect features in a plane, which are related to the concavity-convexity characteristics of surface landforms (Drăguţ and Blaschke, 2006). The Convergence Index measures the degree of flow convergence-divergence for a pixel within the surface model (Dornik et al., 2018). The Terrain Ruggedness Index describes the difference between the height of a pixel compared to its surroundings, representing indexes of local elevation heterogeneity (De Reu et al., 2013; Mieza et al., 2016; Nakileza and Nedala, 2020). All point cloud-based metrics were generated at a 12 cm spatial resolution and using the functions' default parameters.

2.4. Landcover classification

To detect and map coastal areas covered by *R. rugosa*, as well as native vegetation and other landcover classes, we used a training/validation dataset and a supervised Random Forest (RF) classifier (as per Villoslada et al., 2020). The land cover classes used in this study were based on the European Environment Agency's geospatial dataset of European ecosystem types (Chytrý et al., 2020). For this, we considered the following classes of land cover: Marine habitats (MH), Coastal habitats (CH), Grasslands and land dominated by forbs, mosses or lichens (G), *R. rugosa* (RR), Woodland, forest, and other wooded land (W), Arable land and market gardens (A), and Constructed, industrial and other artificial habitats (C). In addition, we included shadows (S) as a separate class.

Contrary to a presence/absence binary classification, this multi-class categorization allows the user to identify classification inaccuracies and attribute the source of error, highlighting classes prone to misclassification. We used the UAV RGB image to digitize 10 training and 10 validation samples per landcover class, per site. Each sample consisted of a circular polygon of 50 cm diameter, which was subsequently used to extract the individual values of all the pixels corresponding to each of the explanatory variables. When digitizing the training/validation dataset, we incorporated *R. rugosa* patches belonging to both clumped and sparse thickets, in order to ensure an adequate coverage of the potential spectral and morphological range of *R. rugosa* shrubs within the study areas.

We performed the landcover classification using a RF machine learning classifier. We chose RF over other algorithms due to its superior performance, its ability to classify spectrally similar plant communities (Villoslada et al., 2022) and capacity to deal with high data dimensionality (Cutler et al., 2007). We used the randomForest package (Liaw and Wiener, 2002) in R v4.1.3, with the RGB VIs and the canopy metrics as input variables. We set the key RF parameters (number of trees and number of randomly selected predictor variables at each split) to 500 and 6 respectively, based on an accuracy assessment through repeated cross-validation.

The resulting maps were validated using the *validateMap* function within the RStoolbox package (Leutner et al., 2017). To validate the overall classification accuracy, we selected the commonly used metrics *overall accuracy* and *F1-score* from caret (Kuhn, 2008) and MLmetrics (Yan, 2016) packages in R, respectively. To evaluate per-class accuracies and detect potential misclassifications between classes, we utilized *sensitivity* (i.e., the rate of true positives) and *specificity* (i.e., the true negative rate in a confusion matrix; Nhu et al., 2020).

2.5. Upscaling

The near-infrared band included in the PlanetScope constellation enables the generation of VIs that are superior to those based solely on RGB bands. We took advantage of this and created a set of ten vegetation indices (Table 1), selected based on their ability to counteract the effect of soil in sparsely vegetated areas (Modified Soil Adjusted Vegetation Index and Soil Adjusted Vegetation Index), robustness in vegetation density, coverage and biomass predictions (Difference Vegetation Index, Green Red Difference Index, Green Difference Index, Normalized Difference Vegetation Index, Green Normalized Vegetation Index and Enhanced Vegetation Index), and good performance in areas characterized by high moisture levels (Green Ratio Vegetation Index) (Villoslada et al., 2022).

In addition to the satellite-derived vegetation indices, we selected two variables related to the autecological preferences of *R. rugosa*: Distance to the coastline and elevation. These co-predictors constitute proxies for salinity, inundation and air humidity, which in turn drive *R. rugosa* distribution (Ööpik et al., 2008). Elevation was derived from the airborne LiDAR datasets acquired by the Estonian Land Board, with a resolution of 1 m per pixel.

To upscale the UAV-derived *R. rugosa* extent to PlanetScope, we used a within-pixel fractional cover approach (Riihimäki et al., 2019; Gränzig et al., 2021; Fraser et al., 2022). In this method, fractional cover is understood as the number of UAV pixels belonging to the vegetation class under study divided by the total number of UAV pixels within a satellite grid cell. Following this rationale, we aggregated the fractional cover of the UAV-derived landcover classes within the PlanetScope pixels. We first converted the PlanetScope raster images to a vector grid, where each vector polygon aligned each raster pixel. We then intersected the polygon grid with the UAV-derived vegetation maps, extracted the area of each landcover class, and calculated the fractional cover of each class. We performed these operations in QGIS Desktop v.3.24.1.

We predicted the fractional cover of *R. rugosa* with an Extreme Gradient Boosting (XGBoost) regression algorithm. XGBoost has consistently outperformed machine and deep learning algorithms in regression problems (Zhang et al., 2019; Zhong et al., 2019), and is known to be robust to noise and class imbalance (Chen and Guestrin, 2016). We built the XGBoost model using the *raster* (Hijmans et al., 2015) and *xgboost* packages (Chen et al., 2019) and fine-tuned the hyperparameters of XGBoost (learning rate, number of trees, minimum number of samples required at a leaf node, maximum depth, the number of features for the best split and *gamma* [γ]) with the *mlr* package (Bischl et al., 2016), using a five-fold cross-validation approach and 100 optimization rounds. To ensure robustness in the upscaling process, we iterated the XGBoost algorithm 50 times and averaged the predictions to produce the final *R. rugosa* fractional cover maps.

We used the VIs derived from the PlanetScope bands and the two autecological variables as co-predictors, and the *R. rugosa* fractional cover within the PlanetScope pixels as the training/validation data. Finally, we randomly split the dataset into one-half for training and one-half for validation. To test the prediction ability of the XGBoost upscaling algorithms, we generated two different models. The first model (*all-sites* model hereinafter) used training data from the seven study sites and predicted *R. rugosa* fractional cover in all sites. The second model (*external validation* model hereinafter) used training data from all sites except Laulasmaa and predicted *R. rugosa* fractional cover along the coastal fringe of Laulasmaa.

We validated the XGBoost regression models using the coefficient of determination (R^2) and the Root Mean Square Error (RMSE) with the *validateMap* function within the RStoolbox package. We used the *Gain* metric to estimate the relative contribution of a feature within the XGBoost algorithm based on the total gain of the feature's splits in the model. Higher gain percentage represents a higher predictive power (Chen et al., 2019).

Table 1
List of vegetation Indices selected to predict *R. rugosa* fractional cover within the PlanetScope pixels. *G*: green band (500–590 nm), *NIR*: near-infrared band (780–860 nm), *R*: red band (590–670 nm).

Vegetation and textural index	Equation	Reference
Chlorophyll vegetation index (CVI)	(NIR/G) × (R/G)	Vincini et al. (2007)
Difference Vegetation Index (DVI)	NIR-αR α = 0.96916	Richardson and Everitt (1992), Maguigan et al. (2016)
2-band Enhanced Vegetation Index (EVI)	2.5 [(NIR-R)/(NIR + 2.4 R + 1)]	Jiang et al. (2008), Jin et al. (2014)
Green Difference Index (GDI)	NIR-R + G	Gianelle and Vescovo (2007)
Green Normalized Vegetation Index (GNDVI)	(NIR-G)/(NIR + G)	Gitelson et al. (1996), Naidoo et al. (2019)
Green-Red Difference Index (GRDI)	(G-R)/(G + R)	Gianelle and Vescovo (2007)
Green Ratio Vegetation Index (GRVI)	NIR/G	Sripada et al. (2006), Naidoo et al. (2019)
Modified Soil Adjusted Vegetation Index (MSAVI)	$0.5*[2*NIR - \sqrt{(2*NIR+1)^2} - 8*(NIR - R)]$	Qi et al. (1994), Jin et al. (2014)
Normalized Difference Vegetation Index (NDVI)	(NIR-R)/(NIR + R)	Rouse et al. (1974)
Soil Adjusted Vegetation Index (SAVI)	[(NIR-R)/(NIR + R + L)](1 + L) L (soil adjustment factor) = 0.5	Huete (1988), Ullah et al. (2012)

3. Results

3.1. UAV-based R. rugosa distribution maps

In the study areas, *R. rugosa* forms thickets along the coastline, primarily in the upper section of the sandy and rocky shores, adjacent to the forest edge (Fig. 2). The degree of encroachment varies between sites, from heavily encroached areas where dense thickets suppress the natural herbaceous vegetation (Laulasmaa), to sparse thickets forming mosaics in the sandy beaches, low scrub and herbaceous vegetation (Rooslepa) (Fig. 2).

The RF classifier yielded high overall accuracies, with values of 0.81 for overall accuracy and 0.75 for F1-score (Table 2). Site-specific accuracies yielded slightly divergent results (Table 2), with the lowest accuracies recorded at Valkla (overall accuracy = 0.74 and F1-score = 0.67) and the highest at Nõva (overall accuracy = 0.85 and F1-score = 0.82) and Pärispea (overall accuracy = 0.89 and F1-score = 0.88). The per-class accuracies showed the ability of RF to predict *R. rugosa*, with a sensitivity of 0.92 and a specificity of 0.96. Similarly, sensitivity and specificity values were high for *R. rugosa* at all sites (Table 3). Generally, specificity was higher than sensitivity for all landcover classes (Table 2). The lowest sensitivity recorded corresponded to arable land (0.20).

Regarding the variable importance, GLCM dissimilarity clearly emerged as a crucial co-predictor in the overall RF landcover classification (Fig. 3) according to the mean decrease in accuracy. A VI (WI) and two canopy metrics (CI and kurtosis of height distribution) also contributed substantially to the performance of the RF algorithm.

3.2. UAV – PlanetScope upscaling

The correspondence between the *R. rugosa* fractional cover values within PlanetScope pixels and the UAV-based predictions highlighted the good performance of the XGBoost algorithm in the *all-sites* model (RMSE = 0.11 and R^2 = 0.70, Table 4). However, per-site accuracies (Table 4; Fig. S1) revealed contrasting results. For instance, sites with a

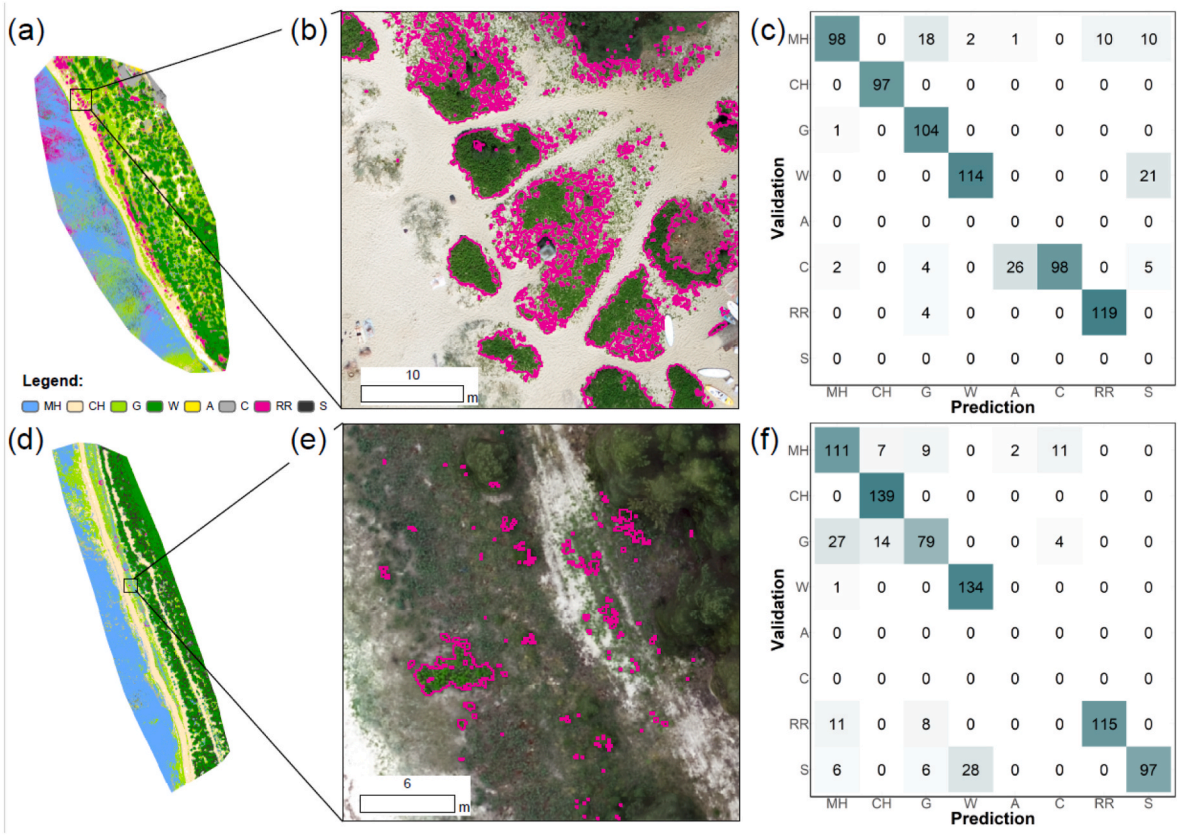

Fig. 2. Random Forest model predictions for the occurrence and distribution of landcover classes at two contrasting locations: Heavily encroached areas at Laulasmaa (a and b) and sparse distribution of *R. rugosa* at Rooslepa (d and e). The confusion matrices of each study site are shown in panels (c and f). MH: Marine habitats; CH: Coastal habitats; G: Grasslands and land dominated by forbs, mosses or lichens; RR: *R. rugosa*; W: Woodland, forest, and other wooded land; A: Arable land and market gardens; C: constructed, industrial and other artificial habitats; S: shadows.

Table 2
Classification accuracies (overall accuracy, 95% confidence interval and F1-score) for the overall classification and each study site using random forest. The table also includes the sensitivity and specificity of the *R. rugosa* classification at each study site.

Site	Overall accuracy	95% CI	F1-score	Sensitivity *R. rugosa*	Specificity *R. rugosa*
Overall classification	0.81	(0.80, 0.82)	0.75	0.92	0.96
Vainupea	0.80	(0.77, 0.82)	0.80	0.87	0.96
Laulasmaa	0.80	(0.77, 0.83)	0.77	0.89	0.94
Neeme	0.82	(0.80, 0.84)	0.74	0.94	0.99
Nõva	0.85	(0.82, 0.87)	0.82	0.96	0.99
Rooslepa	0.82	(0.81, 0.85)	0.73	0.90	1.00
Valkla	0.74	(0.72, 0.76)	0.67	0.97	0.96
Pärispea	0.89	(0.85, 0.90)	0.88	1.00	0.85

Table 3
Per-class accuracy metrics for the overall classification with random forest. MH: Marine habitats; CH: Coastal habitats; G: Grasslands and land dominated by forbs, mosses or lichens; RR: *R. rugosa*; W: Woodland, forest, and other wooded land; A: Arable land and market gardens; C: constructed, industrial and other artificial habitats; S: shadows.

	Landcover classes							
Accuracy metrics	MH	CH	G	**RR**	W	A	C	S
Sensitivity	0.72	0.92	0.68	0.92	0.93	0.20	0.68	0.81
Specificity	0.96	0.98	0.96	0.96	0.99	0.99	0.98	0.96

very low *R. rugosa* coverage such as Nõva and Rooslepa, also presented lower accuracy values (Nõva $R^2 = 0.03$ and Rooslepa $R^2 = 0.25$). The relative contribution of the co-predictors measured by the Gain metric highlighted the role of the autecological variables (Fig. 4). Distance to the coastline and elevation were ranked as the second and third most important variables, with gain scores of 0.12 and 0.10 respectively. The most important variable was the Difference Vegetation Index (DVI), with a gain score of 0.32. Green Ratio Vegetation Index (GRVI) and Modified Soil Adjusted Vegetation Index (MSAVI) were featured as the least important co-predictors within the XGBoost regression algorithm.

Although the upscaling of fractional cover to satellite-level resolution inevitably smooths the outline and pattern of *R. rugosa* thickets, the high GSD of PlanetScope allows the overall shape of the patches to be retained. This is clearly visible in dense thickets, such as those in Viinistu (Fig. 4). Small and sparse individuals, such as those present in the Vainupea area, were also relatively well captured by the XGBoost algorithm.

Regarding the *external validation* model, the RMSE values were equal to those corresponding the *all-sites* model in Laulasmaa (0.18, Fig. 5). However, the R^2 showed considerably lower values for the *external*

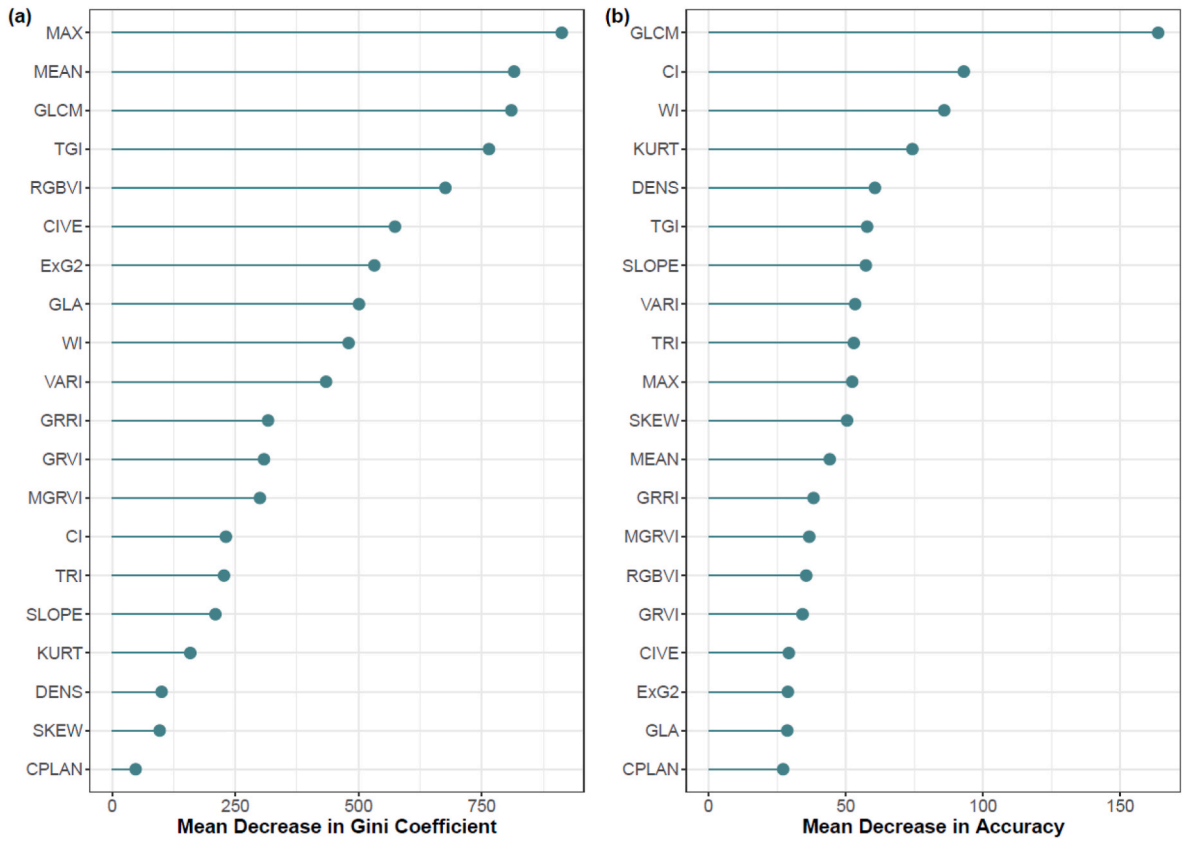

Fig. 3. Contribution of each explanatory variable to the overall performance of the Random Forest classification model for landcover classes. Variable contributions are estimated using Mean Decreased Gini (MDG) (a) and Mean Decreased Accuracy (MDA) (b). Higher MDA and MDG values indicate a higher importance of the input variable in the classification process. MAX: maximum height, MEAN: mean height, DENS: density of points, SKEW: skewness of height distribution, KURT: kurtosis of height distribution, SLOPE: slope of the surface, CI: convergence index, TRI: terrain ruggedness index, CPLAN: plane curvature.

Table 4
Overall and site-specific accuracies for the prediction of *R. rugosa* fractional cover using a XGBoost regression algorithm. RMSE: Root Mean Squared Error, R2: Coefficient of determination, r: Pearson correlation coefficient.

Site	RMSE	R^2
Overall classification	0.11	0.70
Vainupea	0.12	0.60
Laulasmaa	0.14	0.66
Neeme	0.12	0.60
Nõva	0.04	0.03
Rooslepa	0.04	0.25
Valkla	0.10	0.65
Pärispea	0.17	0.74

validation model (0.40). The comparison of both fractional cover maps shows an underestimation of *R. rugosa,* both in terms of extent and fractional cover (Fig. 5).

4. Discussion

In this work we demonstrated the effectiveness of combining UAV-derived RGB images with high GSD multispectral satellite imagery to detect and map the extent of *R. rugosa* in coastal areas. The UAV-satellite fusion methods we present here expand the capabilities of invasive species mapping and monitoring beyond the relatively reduced extents of UAV-surveyed areas, and provides a robust tool for the quantification and management of areas encroached by *R. rugosa.* Moreover, we demonstrate the feasibility of using low-cost RGB sensors, which constitute a highly cost-effective monitoring tool for the often budget-limited environmental agencies.

4.1. UAV-based landcover classification and detection of R. rugosa

The Random Forest model successfully predicted all landcover classes under assessment. Sensitivity and specificity showed a particularly high accuracy for *R. rugosa*, highlighting the robustness of the model in predicting the location and extent of thickets of this invasive shrub. The accuracies we achieved using RGB images as a basis for the model are comparable to those obtained in similar environments using multispectral (Marzialetti et al., 2021) and hyperspectral sensors (Kattenborn et al., 2019), highlighting the feasibility of low-cost sensors for mapping and monitoring invasive plant species. We highlight the benefit of including textural indices and canopy metrics derived from 3D point clouds among the model co-predictors, in order to increase prediction accuracies. This is supported by the Random Forest variable importance metrics (mean decrease in Gini coefficient and mean decrease in accuracy), which included GLCM, maximum height, mean height, and kurtosis of the height distribution among the key co-predictors in terms of model performance. Our findings are consistent with previous publications that highlight the need to complement spectral information with canopy structural data such as those derived from photogrammetric products (Kattenborn et al., 2019; Lopatin et al., 2019, 2019de Lima et al., 2022) and laser scanning (Hantson et al., 2012; da Silva et al., 2022). This may be especially true when the source of spectral information are red, green and blue bands. In the absence of more sensitive spectral ranges such as the near-infrared and red-edge bands, RGB-based vegetation indices may fail to distinguish chromatically-similar vegetation classes. In this case, canopy metrics provide the necessary information to discern canopy structures associated with different species.

We found minor differences between sites regarding the sensitivity and specificity of classification for *R. rugosa*. We attribute the

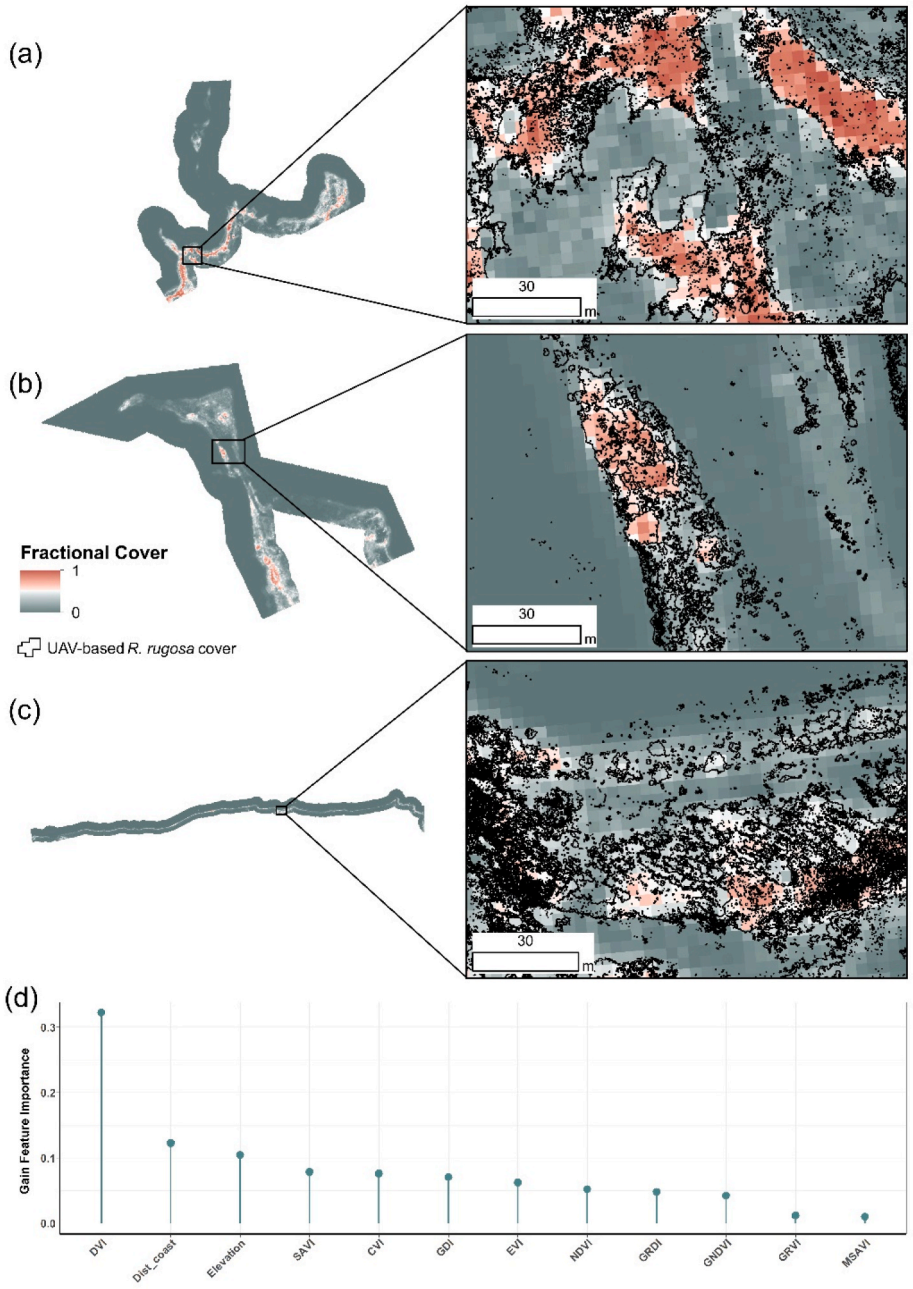

Fig. 4. XGBoost model predictions for *R. rugosa* fractional cover within PlanetScope pixels at sites (a) Viinistu, (b) Neeme and (c) Vainupea, along with the contribution of each explanatory variable using the Gain metric (d).

consistency in classification performance to *R. rugosa*'s physiognomy. The dense, monospecific thickets are characterized by purer and more homogeneous spectral signatures compared with other vegetation types. The performance of classifiers benefits from the spectral homogeneity among the samples of this species, since classification accuracies are usually hindered by an increase in species diversity (Villoslada et al., 2020; da Silva et al., 2022). Moreover, previous research demonstrated that the ability to recognize woody species improves with patch size (Hantson et al., 2012). The negative effect of spectrum mixing was observed in locations where *R. rugosa* occurred in small patches, such as in Rooslepa (Fig. 2), which resulted in a reduced ability to detect this species. We argue that *R. rugosa* thickets and woodlands are characterized by more homogenous covers and therefore reduced spectral diversity compared to grasslands or gardens (Wang et al., 2018; Conti et al., 2021). Consequently, the combination of different data types for classifying spectrally similar vegetation types compensated for the weakness of RGB indices to describe vegetation structure and, thus, enhance its accuracy, which is consistent with previous publications (Hantson et al., 2012; Beyer et al., 2019; da Silva et al., 2022).

4.2. UAV-PlanetScope upscaling of R. rugosa fractional cover

The XGBoost fractional cover predictions exhibited a high degree of agreement with the UAV-derived maps of *R. rugosa* (RMSE = 0.11, R^2 = 0.70), similar to those achieved in recent publications (Marzialetti et al., 2022). These results confirm the ability of UAV data to provide robust training and validation information, which would have otherwise required a vast amount of time and resources using field inventory procedures. Moreover, satellite-based predictions of *R. rugosa* fractional cover provides a robust tool to extend the scope of assessment beyond

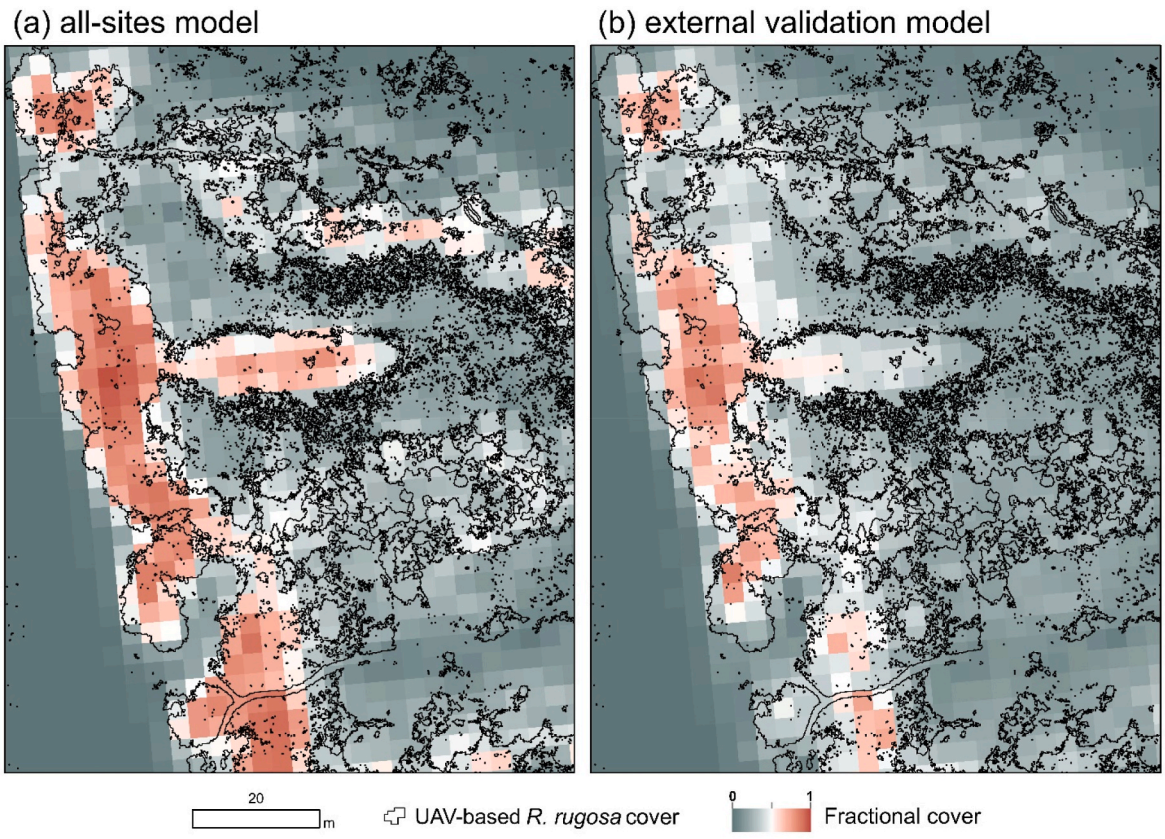

Fig. 5. Comparison of XGBoost model predictions for *R. rugosa* fractional cover in Laulasmaa using two different training datasets: (a) *all-sites* model, and (b) *external validation* model.

UAV-surveyed areas, therefore increasing the efficiency of invasive species monitoring campaigns.

In this study, we undertook an exhaustive algorithm performance assessment by addressing site-specific accuracies and generating an external validation model. Overall accuracy assessments provide a comparable estimate of model performance, but fail to reveal potential pitfalls and associated sources of error. The per-site accuracy assessment unveiled considerable differences in the performance of the XGBoost model. The lowest accuracies were recorded at Nõva (RMSE = 0.04 and $R^2 = 0.03$) and Rooslepa (RMSE = 0.04 and $R^2 = 0.25$). These two sites are characterized by a very low coverage of *R. rugosa*, which appears as small and sparse shrubs, rarely forming thickets. Despite the very high GSD of the PlanetScope satellites, the spectral signature of small-sized *R. rugosa* individuals (in some cases down to ca 30 cm wide) may be mixed with the surrounding landcover. In contrast, areas where *R. rugosa* forms dense thickets such as Neeme and Valkla showed higher prediction accuracies (RMSE = 0.12 and RMSE = 0.10 respectively). Sub-pixel spectral and structural heterogeneity are well recognized causes for decreased accuracies in classification and regression algorithms (Villoslada et al., 2020; Yang et al., 2020; Burchard-Levine et al., 2021). Re-balancing the training dataset through synthetic training data generation and under-sampling (Branco et al., 2017) could potentially improve the accuracy in sites with small and sparse thickets.

We further tested the robustness of the upscaling approach using an *external validation* model; that is, a XGBoost algorithm trained with data from all study sites except the one it was tested on (Laulasmaa). As suggested by Kattenborn et al. (2021), an optimal validation approach should include fully independent validation data that has not been inputted in the model before. Here, we chose an entirely external location for this validation, to ensure we could assess the accuracy of fractional cover predictions under different spectral and environmental characteristics. As we expected, the accuracies of the *external validation* model were lower than those of the *all-sites* model (RMSE = 0.18 and $R^2 = 0.40$). Fig. 5 shows how the *external validation* model tends to underestimate and homogenize *R. rugosa* fractional cover in comparison to the *all-sites* model. We attribute the lower accuracies to two different aspects. Firstly, the XGBoost model was not trained with data from Laulasmaa and therefore did not capture the local spectral and morphological variability, resulting in a lower R^2 value that indicated a reduced ability to explain the variance in *R. rugosa* fractional cover. A second source of error could be attributed to the PlanetScope constellation. The revisit times and patterns of the PlanetScope constellation are highly complex and geographically variable (Roy et al., 2021). This, combined with lighting inconsistencies and sensor variations within the constellation (Csillik et al., 2020) render geographical extrapolations of models challenging. Despite the low R^2 values, an RMSE of 0.18 indicates the feasibility of the method to extrapolate *R. rugosa* fractional cover predictions beyond the sites used as a source of training data. However, the per-site accuracies and underestimations observed in Fig. 5 suggest that geographical extrapolations of the model may not be achievable in sites characterized by early encroachment stages.

Regarding variable importance, the Gain metric highlighted the role of the Difference Vegetation Index (DVI) in predicting *R. rugosa* fractional cover. It has been previously shown that DVI is highly sensitive to above ground biomass in wetland ecosystems (Gitelson, 2004; Maguigan et al., 2016). Distance to the shoreline and elevation scored as the second and third most important variables for the XGBoost performance. Once again, this supports the notion that spectral data alone does not capture the geophysical variables and autecological preferences that explain plant species distributions (Villoslada et al., 2021). We argue that distance to the shoreline and elevation are closely related to moisture and salinity levels (Ward et al. 2014, 2016) and that, these, in turn, partly drive the distribution of *R. rugosa* (Ööpik et al., 2008). Previous studies have shown that even in the brackish coastal

environments of Estonia, microtopography is strongly associated with salinity and the distribution of moisture gradients (Ward et al., 2016; Villoslada et al., 2021).

4.3. Implications for management

Invasive plant species can cause both severe biodiversity and economic losses. In Europe, the economic impact has been estimated at ca EUR 12 billion per year (Lipa, 2013). Despite global efforts in eradication (Weidlich et al., 2020), efficient management strategies are hindered by delayed early detection (Tataridas et al., 2022), accurate quantification, and insufficient post-eradication monitoring (Foxcroft et al., 2017). Here, we propose a framework that supplies spatial information relevant for *R. rugosa* management at two scales. At the local scale, the UAV-based models provide highly accurate estimations that allow for early detection, quantification, and post-restoration monitoring. As indicated by Villalobos Perna et al. (2023), UAVs may play a crucial role in areas characterized by a low invasion degree, as evidenced by our results (Fig. 1). At the regional scale, the fusion of UAV and PlanetScope data serves as a tool for estimation of *R. rugosa* coverage.

The RGB-based framework we propose in this study yielded accuracies comparable to those achieved with multispectral and hyperspectral sensors (Marzialetti et al., 2021; Kattenborn et al., 2019), therefore allowing for cost-efficient mapping of invasive plants species using consumer grade UAVs. This is of critical importance for environmental agencies and other governmental bodies, where survey resources and personnel are often scarce (Yemshanov et al., 2022). In this regard, the advantages of semi-automatic detection, based on machine learning algorithms over manual delineation or field inventories are evident. Moreover, the robust results of the UAV–based classification in areas with very low and fragmented coverage of *R. rugosa* suggest that this approach could be transferred to other invasive plant species in coastal areas worldwide, such as those belonging to the *Spartina*, *Phragmites*, *Sporobolus*, *Acacia,* and *Carpobrotus* genera (Wan et al., 2014; Abeysinghe et al., 2019; Villalobos Perna et al., 2023).

5. Conclusions

In this study we presented a framework to map the extent of *Rosa rugosa* in coastal areas in Estonia combining UAV RGB images and PlanetScope multispectral images. At the UAV level, the combination of RGB-based vegetation indices and canopy metrics achieved very high mapping accuracies, constituting a highly cost-effective tool for agencies involved in the eradication of invasive plant species. UAVs equipped with inexpensive RGB sensors can achieve accuracies similar to those carrying multispectral cameras. Upscaling the UAV-derived *R. rugosa* presence/absence to PlanetScope derived fractional cover provided a high overall accuracy of the prediction model. However, we strongly recommend addressing site-specific accuracies, in order to identify potential modelling pitfalls particularly in sites with low and fragmented cover of invasives. This highlights the need to incorporate training data representing a wide range of encroachment stages and move beyond single-site assessments in order to operationalize UAV-satellite upscaling approaches. While the majority of publications use in-situ training data, we consider that external training/validation models are fundamental to fully understand the predictive capabilities of machine learning algorithms. Our external training/validation model yielded, as expected, lower accuracies than the XGBoost model trained with in-situ data, further reinforcing the importance of diverse training datasets. We also note that there are some issues with using the PlanetScope constellation due to reproducibility as a result of the sensor diversity between satellites. In conclusion, we regard the methods presented in this paper as an important contribution to the ongoing efforts to control invasive plant species worldwide. UAVs in combination with satellite data provide an important foundation for improving estimations of invasive species coverage and targeted eradication programs.

Credit author statement

Thaisa F. Bergamo: collected and analyzed the data, and wrote the manuscript; Raul S. de Lima: collected and analyzed the data, and wrote the manuscript; Tiiu Kull: wrote the manuscript; Raymond D. Ward: wrote and revised the manuscript; Kalev Sepp: revised the manuscript; Miguel Villoslada: conceptualized and wrote the manuscript, analyzed the data, supervised, and acquired funding.

Declaration of competing interest

The authors declare the following financial interests/personal relationships which may be considered as potential competing interests: Thaisa Fernandes Bergamo reports financial support was provided by Estonian Research Council.

Data availability

Data will be made available on request.

Acknowledgements

The authors would like to express their gratitude to the Estonian Research Council for funding this work. This study was supported by the Estonian Research Council (EAG204). Likewise, the authors would like to thank the Ecosystem Services Partnership for the opportunity to present this work.

Appendix A. Supplementary data

Supplementary data to this article can be found online at https://doi.org/10.1016/j.jenvman.2023.117693.

References

Abeysinghe, T., Simic Milas, A., Arend, K., Hohman, B., Reil, P., Gregory, A., Vázquez-Ortega, A., 2019. Mapping invasive Phragmites australis in the old woman creek estuary using UAV remote sensing and machine learning classifiers. Rem. Sens. 11, 1380. https://doi.org/10.3390/rs11111380.

Anderson, H.B., Nilsen, L., Tømmervik, H., Karlsen, S.R., Nagai, S., Cooper, E.J., 2016. Using ordinary digital cameras in place of near-infrared sensors to derive vegetation indices for phenology studies of High Arctic vegetation. Rem. Sens. 8 (10), 847. https://doi.org/10.3390/rs8100847.

Beyer, F., Jurasinski, G., Couwenberg, J., Grenzdörffer, G., 2019. Multisensor data to derive peatland vegetation communities using a fixed-wing unmanned aerial vehicle. Int. J. Rem. Sens. 40 (24), 9103–9125. https://doi.org/10.1080/01431161.2019.1580825.

Bischl, B., Lang, M., Kotthoff, L., Schiffner, J., Richter, J., Studerus, E., et al., 2016. Mlr: machine learning in R. J. Mach. Learn. Res. 17 (1), 5938–5942.

Branco, P., Torgo, L., Ribeiro, R.P., 2017. SMOGN: a pre-processing approach for imbalanced regression. In: First International Workshop on Learning with Imbalanced Domains: Theory and Applications. PMLR, pp. 36–50.

Brenning, A., Bangs, D., Becker, M., Schratz, P., Polakowski, F., 2018. Package 'RSAGA'. The Comprehensive R Archive Network. https://CRAN. R-project. org/package=RSAGA.

Bruun, H.H., 2006. Prospects for biocontrol of invasive Rosa rugosa. BioControl 51 (2), 141–181. https://doi.org/10.1007/s10526-005-6757-6.

Burchard-Levine, V., Nieto, H., Riaño, D., Migliavacca, M., El-Madany, T.S., Guzinski, R., et al., 2021. The effect of pixel heterogeneity for remote sensing based retrievals of evapotranspiration in a semi-arid tree-grass ecosystem. Remote Sens. Environ. 260, 112440 https://doi.org/10.1016/j.rse.2021.112440.

Caplat, P., Coutts, S., Buckley, Y.M., 2012. Modeling population dynamics, landscape structure, and management decisions for controlling the spread of invasive plants. Ann. N. Y. Acad. Sci. 1249 (1), 72–83. https://doi.org/10.1111/j.1749-6632.2011.06313.x.

Carboni, M., Santoro, R., Acosta, A.T.R., 2010. Are some communities of the coastal dune zonation more susceptible to alien plant invasion? J. Plant Ecol. 3 (2), 139–147. https://doi.org/10.1093/jpe/rtp037.

Chen, T., Guestrin, C., 2016. Xgboost: a scalable tree boosting system. In: Proceedings of the 22nd Acm Sigkdd International Conference on Knowledge Discovery and Data Mining, pp. 785–794. https://doi.org/10.1145/2939672.2939785.

Chen, T., He, T., Benesty, M., Khotilovich, V., 2019. Package 'xgboost'. R version, p. 90.

Cheney, C., Esler, K.J., Foxcroft, L.C., van Wilgen, N.J., McGeoch, M.A., 2018. The impact of data precision on the effectiveness of alien plant control programmes: a case study from a protected area. Biol. Invasions 20 (11), 3227–3243. https://doi.org/10.1007/s10530-018-1770-8.

Chytrý, M., Tichý, L., Hennekens, S.M., Knollová, I., Janssen, J.A., Rodwell, J.S., et al., 2020. EUNIS Habitat Classification: expert system, characteristic species combinations and distribution maps of European habitats. Appl. Veg. Sci. 23 (4), 648–675. https://doi.org/10.1111/avsc.12519.

Conti, L., Malavasi, M., Galland, T., Komárek, J., Lagner, O., Carmona, C.P., et al., 2021. The relationship between species and spectral diversity in grassland communities is mediated by their vertical complexity. Appl. Veg. Sci. 24 (3) https://doi.org/10.1111/avsc.12600.

Csillik, O., Kumar, P., Asner, G.P., 2020. Challenges in estimating tropical forest canopy height from planet dove imagery. Rem. Sens. 12 (7), 1160. https://doi.org/10.3390/rs12071160.

Cutler, D.R., Edwards Jr., T.C., Beard, K.H., Cutler, A., Hess, K.T., Gibson, J., Lawler, J.J., 2007. Random forests for classification in ecology. Ecology 88 (11), 2783–2792. https://doi.org/10.1890/07-0539.1.

Da Silva, A.R., Demarchi, L., Sikorska, D., Sikorski, P., Archiciński, P., Jóźwiak, J., Chormański, J., 2022. Multi-source remote sensing recognition of plant communities at the reach scale of the Vistula River, Poland. Ecol. Indicat. 142, 109160 https://doi.org/10.1016/j.ecolind.2022.109160.

De Lima, R.S., Li, K.Y., Vain, A., Lang, M., Bergamo, T.F., Kokamägi, K., et al., 2022. The potential of optical UAS data for predicting surface soil moisture in a peatland across time and sites. Rem. Sens. 14 (10), 2334. https://doi.org/10.3390/rs14102334.

De Reu, J., Bourgeois, J., Bats, M., Zwertvaegher, A., Gelorini, V., De Smedt, P., Chu, W., Antrop, M., De Maeyer, P., Finke, P., Van Meirvenne, M., Verniers, J., Crombé, P., 2013. Application of the topographic position index to heterogeneous landscapes. Geomorphology 186, 39–49. https://doi.org/10.1016/j.geomorph.2012.12.015.

De Swaef, T., Maes, W.H., Aper, J., Baert, J., Cougnon, M., Reheul, D., et al., 2021. Applying RGB-and thermal-based vegetation indices from UAVs for high-throughput field phenotyping of drought tolerance in forage grasses. Rem. Sens. 13 (1), 147. https://doi.org/10.3390/rs13010147.

Díaz-Ramírez, J., 2021. Machine learning and deep learning. Ingeniare 29 (2), 182–183. https://doi.org/10.4067/S0718-33052021000200180.

Dong, Z., Wang, N., Liu, J., Xie, J., Han, J., 2021. Combination of machine learning and VIRS for predicting soil organic matter. J. Soils Sediments 21 (7), 2578–2588. https://doi.org/10.1007/s11368-021-02977-0.

Dornik, A., Drăguţ, L., Urdea, P., 2018. Classification of soil types using geographic object-based image analysis and random forests. Pedosphere 28 (6), 913–925. https://doi.org/10.1016/S1002-0160(17)60377-1.

Dos Reis, A.A., Werner, J.P., Silva, B.C., Figueiredo, G.K., Antunes, J.F., Esquerdo, J.C., et al., 2020. Monitoring pasture aboveground biomass and canopy height in an integrated crop–livestock system using textural information from PlanetScope imagery. Rem. Sens. 12 (16), 2534. https://doi.org/10.3390/rs12162534.

Drăguţ, L., Blaschke, T., 2006. Automated classification of landform elements using object-based image analysis. Geomorphology 81 (3–4), 330–344. https://doi.org/10.1016/j.geomorph.2006.04.013.

Francini, S., McRoberts, R.E., Giannetti, F., Mencucci, M., Marchetti, M., Scarascia Mugnozza, G., Chirici, G., 2020. Near-real time forest change detection using PlanetScope imagery. European Journal of Remote Sensing 53 (1), 233–244. https://doi.org/10.1080/22797254.2020.1806734.

Fraser, R.H., Pouliot, D., van der Sluijs, J., 2022. UAV and high resolution satellite mapping of forage lichen (cladonia spp.) in a rocky Canadian shield landscape. Can. J. Rem. Sens. 48 (1), 5–18. https://doi.org/10.1080/07038992.2021.1908118.

Frazier, A.E., Hemingway, B.L., 2021. A technical review of planet smallsat data: practical considerations for processing and using PlanetScope imagery. Rem. Sens. 13 (19), 3930. https://doi.org/10.3390/rs13193930.

Foxcroft, L.C., Pyšek, P., Richardson, D.M., Genovesi, P., MacFadyen, S., 2017. Plant invasion science in protected areas: progress and priorities. Biol. Invasions 19, 1353–1378. https://doi.org/10.1007/s10530-016-1367-z.

Gianelle, D., Vescovo, L., 2007. Determination of green herbage ratio in grasslands using spectral reflectance. Methods and ground measurements. Int. J. Rem. Sens. 28 (5), 931–942. https://doi.org/10.1080/01431160500196398.

Gitelson, A.A., 2004. Wide dynamic range vegetation index for remote quantification of biophysical characteristics of vegetation. J. Plant Physiol. 161 (2), 165–173.

Gitelson, A.A., Kaufman, Y.J., Merzlyak, M.N., 1996. Use of a green channel in remote sensing of global vegetation from EOS-MODIS. Rem. Sens. Environ. 58 (3), 289–298. https://doi.org/10.1016/S0034-4257(96)00072-7.

Gränzig, T., Fassnacht, F.E., Kleinschmit, B., Förster, M., 2021. Mapping the fractional coverage of the invasive shrub Ulex europaeus with multi-temporal Sentinel-2 imagery utilizing UAV orthoimages and a new spatial optimization approach. Int. J. Appl. Earth Obs. Geoinf. 96 (December 2020) https://doi.org/10.1016/j.jag.2020.102281.

Guijarro, M., Pajares, G., Riomoros, I., Herrera, P.J., Burgos-Artizzu, X.P., Ribeiro, A., 2011. Automatic segmentation of relevant textures in agricultural images. Comput. Electron. Agric. 75 (1), 75–83. https://doi.org/10.1016/j.compag.2010.09.013.

Hantson, W., Kooistra, L., Slim, P.A., 2012. Mapping invasive woody species in coastal dunes in the N etherlands: a remote sensing approach using LIDAR and high-resolution aerial photographs. Appl. Veg. Sci. 15 (4), 536–547. https://doi.org/10.1111/j.1654-109X.2012.01194.x.

Haubrock, P.J., Turbelin, A.J., Cuthbert, R.N., Novoa, A., Taylor, N.G., Angulo, E., et al., 2021. Economic costs of invasive alien species across Europe. NeoBiota 67, 153–190. https://doi.org/10.3897/neobiota.67.58196.

Hijmans, R.J., Van Etten, J., Cheng, J., Mattiuzzi, M., Sumner, M., Greenberg, J.A., et al., 2015. Package 'raster'. R Package, p. 734.

Huete, A.R., 1988. A soil-adjusted vegetation index (SAVI). Rem. Sens. Environ. 25 (3), 295–309. https://doi.org/10.1016/0034-4257(88)90106-X.

Hussain, M., Chen, D., Cheng, A., Wei, H., Stanley, D., 2013. Change detection from remotely sensed images: from pixel-based to object-based approaches. ISPRS J. Photogrammetry Remote Sens. 80, 91–106. https://doi.org/10.1016/j.isprsjprs.2013.03.006.

James, K., Bradshaw, K., 2020. Detecting plant species in the field with deep learning and drone technology. Methods Ecol. Evol. 11 (11), 1509–1519. https://doi.org/10.1111/2041-210X.13473.

Jiang, Z., Huete, A.R., Didan, K., Miura, T., 2008. Development of a two-band enhanced vegetation index without a blue band. Rem. Sens. Environ. 112 (10), 3833–3845. https://doi.org/10.1016/j.rse.2008.06.006.

Jin, Y., Yang, X., Qiu, J., Li, J., Gao, T., Wu, Q., et al., 2014. Remote sensing-based biomass estimation and its spatio-temporal variations in temperate grassland, Northern China. Rem. Sens. 6 (2), 1496–1513. https://doi.org/10.3390/rs6021496.

Jordan, N.R., Larson, D.L., Huerd, S.C., 2008. Soil modification by invasive plants: effects on native and invasive species of mixed-grass prairies. Biol. Invasions 10 (2), 177–190. https://doi.org/10.1007/s10530-007-9121-1.

Joyce, K.E., Anderson, K., Bartolo, R.E., 2021. Of course we fly unmanned—we're women. Drones 5 (1), 21. https://doi.org/10.3390/drones5010021.

Junk, W.J., da Cunha, C.N., 2012. Pasture clearing from invasive woody plants in the Pantanal: a tool for sustainable management or environmental destruction? Wetl. Ecol. Manag. 20 (2), 111–122. https://doi.org/10.1007/s11273-011-9246-y.

Kattenborn, T., Leitloff, J., Schiefer, F., Hinz, S., 2021. Review on convolutional neural networks (CNN) in vegetation remote sensing. ISPRS J. Photogrammetry Remote Sens. 173, 24–49.

Kattenborn, T., Lopatin, J., Förster, M., Braun, A.C., Fassnacht, F.E., 2019. UAV data as alternative to field sampling to map woody invasive species based on combined Sentinel-1 and Sentinel-2 data. Rem. Sens. Environ. 227, 61–73. https://doi.org/10.1016/j.rse.2019.03.025.

Kelager, A., Pedersen, J.S., Bruun, H.H., 2013. Multiple introductions and no loss of genetic diversity: invasion history of Japanese Rose, Rosa rugosa, in Europe. Biol. Invasions 15 (5), 1125–1141. https://doi.org/10.1007/s10530-012-0356-0.

Kemper, H., Kemper, G., Klaumuenzner, T., 2022. Soil erosion calculation using aerial images based dtm in a cross border vinery region. International Archives of the Photogrammetry, Remote Sensing and Spatial Information Sciences - ISPRS Archives 43 (B2–2022), 1041–1046. https://doi.org/10.5194/isprs-archives-XLIII-B2-2022-1041-2022.

Klápště, P., Fogl, M., Barták, V., Gdulová, K., Urban, R., Moudrý, V., 2020. Sensitivity analysis of parameters and contrasting performance of ground filtering algorithms with UAV photogrammetry-based and LiDAR point clouds. International Journal of Digital Earth 1–23. https://doi.org/10.1080/17538947.2020.1791267, 0(0).

Kuhn, M., 2008. Building predictive models in R using the caret package. J. Stat. Software 28, 1–26. https://doi.org/10.18637/jss.v028.i05.

Kukk, T., 1999. Eesti Taimestik. Teaduste Akadeemia Kirjastus.

Kunttu, P., Kunttu, S.-M., 2019. New records of the invasive alien Rosa rugosa (rosaceae) in the archipelago sea national Park , SW Finland. Memo. Soc. Fauna Flora Fenn. 95, 81–88.

Lake, T.A., Briscoe Runquist, R.D., Moeller, D.A., 2022. Deep learning detects invasive plant species across complex landscapes using Worldview-2 and Planetscope satellite imagery. Remote Sensing in Ecology and Conservation. https://doi.org/10.1002/rse2.288.

Lee, D.G., Shin, Y.H., Lee, D.C., 2020. Land cover classification using SegNet with slope, aspect, and multidirectional shaded relief images derived from digital surface model. J. Sens. https://doi.org/10.1155/2020/8825509, 2020.

Lehmann, J.R.K., Prinz, T., Ziller, S.R., Thiele, J., Heringer, G., Meira-Neto, J.A.A., Buttschardt, T.K., 2017. Open-source processing and analysis of aerial imagery acquired with a low-cost Unmanned Aerial System to support invasive plant management. Front. Environ. Sci. 5 (JUL), 1–16. https://doi.org/10.3389/fenvs.2017.00044.

Leutner, B., Horning, N., Leutner, M.B., 2017. Package 'RStoolbox'. R Foundation for Statistical Computing. Version 0.1.

Liaw, A., Wiener, M., 2002. Classification and regression by randomForest. R. News 2 (3), 18–22.

Lipa, J.J., 2013. The Impacts of Invasive Alien Species in Europe. European Environmental Agency Technical, ISBN 978-92-9213-345-0, p. 155. Report No. 16/2012 Anonymous 2012. ISSN 1725-2237.

Lopatin, J., Dolos, K., Kattenborn, T., Fassnacht, F.E., 2019. How canopy shadow affects invasive plant species classification in high spatial resolution remote sensing. Remote Sensing in Ecology and Conservation 5 (4), 302–317. https://doi.org/10.1002/rse2.109.

Mafanya, M., Tsele, P., Botai, J., Manyama, P., Swart, B., Monate, T., 2017. Evaluating pixel and object based image classification techniques for mapping plant invasions from UAV derived aerial imagery: harrisia pomanensis as a case study. ISPRS J. Photogrammetry Remote Sens. 129, 1–11. https://doi.org/10.1016/j.isprsjprs.2017.04.009.

Maguigan, M., Rodgers, J., Dash, P., Meng, Q., 2016. Assessing net primary production in montane wetlands from proximal, airborne, and satellite remote sensing. Adv. Rem. Sens. 5 (2), 118–130. https://doi.org/10.4236/ars.2016.52010.

Mao, P., Ding, J., Jiang, B., Qin, L., Qiu, G.Y., 2022. How can UAV bridge the gap between ground and satellite observations for quantifying the biomass of desert shrub community? ISPRS J. Photogrammetry Remote Sens. 192, 361–376. https://doi.org/10.1016/j.isprsjprs.2022.08.021.

Marcial-Pablo, M.D.J., Gonzalez-Sanchez, A., Jimenez-Jimenez, S.I., Ontiveros-Capurata, R.E., Ojeda-Bustamante, W., 2019. Estimation of vegetation fraction using

RGB and multispectral images from UAV. Int. J. Rem. Sens. 40 (2), 420–438. https://doi.org/10.1080/01431161.2018.1528017.
Martin, F.M., Müllerová, J., Borgniet, L., Dommanget, F., Breton, V., Evette, A., 2018. Using single- and multi-date UAV and satellite imagery to accurately monitor invasive knotweed species. Rem. Sens. 10 (10) https://doi.org/10.3390/rs10101662.
Marzialetti, F., Frate, L., De Simone, W., Frattaroli, A.R., Acosta, A.T.R., Carranza, M.L., 2021. Unmanned Aerial Vehicle (UAV)-based mapping of Acacia saligna invasion in the Mediterranean coast. Rem. Sens. 13 (17), 3361. https://doi.org/10.3390/rs13173361.
Menkis, A., Ihrmark, K., Stenlid, J., Vasaitis, R., 2014. Root-associated fungi of Rosa rugosa grown on the frontal dunes of the Baltic Sea coast in Lithuania. Microb. Ecol. 67 (4), 769–774. https://doi.org/10.1007/s00248-013-0351-8.
Mieza, M.S., Cravero, W.R., Kovac, F.D., Bargiano, P.G., 2016. Delineation of site-specific management units for operational applications using the topographic position index in La Pampa, Argentina. Comput. Electron. Agric. 127, 158–167. https://doi.org/10.1016/j.compag.2016.06.005.
Naidoo, L., Van Deventer, H., Ramoelo, A., Mathieu, R., Nondlazi, B., Gangat, R., 2019. Estimating above ground biomass as an indicator of carbon storage in vegetated wetlands of the grassland biome of South Africa. Int. J. Appl. Earth Obs. Geoinf. 78, 118–129. https://doi.org/10.1016/j.jag.2019.01.021.
Nakileza, B.R., Nedala, S., 2020. Topographic influence on landslides characteristics and implication for risk management in upper Manafwa catchment, Mt Elgon Uganda. Geoenvironmental Disasters 7 (1). https://doi.org/10.1186/s40677-020-00160-0.
Neuville, R., Bates, J.S., Jonard, F., 2021. Estimating forest structure from UAV-mounted LiDAR point cloud using machine learning. Rem. Sens. 13 (3), 1–19. https://doi.org/10.3390/rs13030352.
Nhu, V.H., Mohammadi, A., Shahabi, H., Ahmad, B.B., Al-Ansari, N., Shirzadi, A., et al., 2020. Landslide susceptibility mapping using machine learning algorithms and remote sensing data in a tropical environment. Int. J. Environ. Res. Publ. Health 17 (14), 4933. https://doi.org/10.3390/ijerph17144933.
Nota, E.W., Nijland, W., de Haas, T., 2022. Improving UAV-SfM time-series accuracy by co-alignment and contributions of ground control or RTK positioning. Int. J. Appl. Earth Obs. Geoinf. 109 (April), 102772 https://doi.org/10.1016/j.jag.2022.102772.
Ouyang, Z.T., Zhang, M.Q., Xie, X., Shen, Q., Guo, H.Q., Zhao, B., 2011. A comparison of pixel-based and object-oriented approaches to VHR imagery for mapping saltmarsh plants. Ecol. Inf. 6 (2), 136–146. https://doi.org/10.1016/j.ecoinf.2011.01.002.
Ööpik, M., Kukk, T., Kull, K., Kull, T., 2008. The Importance of Human Mediation in Species Establishment: Analysis of the Alien Flora of Estonia.
Papp, L., van Leeuwen, B., Szilassi, P., Tobak, Z., Szatmári, J., Árvai, M., Mészáros, J., Pásztor, L., 2021. Monitoring invasive plant species using hyperspectral remote sensing data. Land 10 (1), 1–18. https://doi.org/10.3390/land10010029.
Pardini, E.A., Vickstrom, K.E., Knight, T.M., 2015. Early successional microhabitats allow the persistence of endangered plants in coastal sand dunes. PLoS One 10 (4), 1–15. https://doi.org/10.1371/journal.pone.0119567.
Park, Y., Guldmann, J.M., 2020. Measuring continuous landscape patterns with Gray-Level Co-Occurrence Matrix (GLCM) indices: an alternative to patch metrics? Ecol. Indicat. 109, 105802 https://doi.org/10.1016/j.ecolind.2019.105802.
Pickart, A.J., Miller, L.M., Duebendorfer, T.E., 1998. Yellow bush lupine invasion in northern California coastal dunes I. Ecological impacts and manual restoration techniques. Restor. Ecol. 6 (1), 59–68. https://doi.org/10.1046/j.1526-100x.1998.00618.x.
Qi, J., Chehbouni, A., Huete, A.R., Kerr, Y.H., Sorooshian, S., 1994. A modified soil adjusted vegetation index. Rem. Sens. Environ. 48 (2), 119–126. https://doi.org/10.1016/0034-4257(94)90134-1.
Richardson, A.J., Everitt, J.H., 1992. Using spectral vegetation indices to estimate rangeland productivity. Geocarto Int. 7 (1), 63–69. https://doi.org/10.1080/10106049209354353.
Riihimäki, H., Luoto, M., Heiskanen, J., 2019. Estimating fractional cover of tundra vegetation at multiple scales using unmanned aerial systems and optical satellite data. Remote Sens. Environ. 224, 119–132. https://doi.org/10.1016/j.rse.2019.01.030.
Rouse, J.W., Haas, R.H., Schell, J.A., Deering, D.W., 1974. Monitoring vegetation systems in the great plains with ERTS proceeding. In: Third Earth Reserves Technology Satellite Symposium, Greenbelt: NASA SP-351, 30103017.
Roussel, J.R., Auty, D., Coops, N.C., Tompalski, P., Goodbody, T.R., Meador, A.S., et al., 2020. lidR: an R package for analysis of Airborne Laser Scanning (ALS) data. Remote Sens. Environ. 251, 112061.
Roy, D.P., Huang, H., Houborg, R., Martins, V.S., 2021. A global analysis of the temporal availability of PlanetScope high spatial resolution multi-spectral imagery. Remote Sens. Environ. 264, 112586 https://doi.org/10.1016/j.rse.2021.112586.
Sampedro, C., Mena, C.F., 2018. Remote sensing of invasive species in the galapagos islands: comparison of pixel-based, principal component, and object-oriented image classification approaches. Understanding Invasive Species in the Galapagos Islands: From the Molecular to the Landscape 155–174. https://doi.org/10.1007/978-3-319-67177-2_9.
Shiferaw, H., Bewket, W., Eckert, S., 2019. Performances of machine learning algorithms for mapping fractional cover of an invasive plant species in a dryland ecosystem. Ecol. Evol. 9 (5), 2562–2574. https://doi.org/10.1002/ece3.4919.
Smith, M.W., Carrivick, J.L., Quincey, D.J., 2016. Structure from motion photogrammetry in physical geography. Prog. Phys. Geogr. 40 (2), 247–275. https://doi.org/10.1177/0309133315615805.
Sripada, R.P., Heiniger, R.W., White, J.G., Meijer, A.D., 2006. Aerial color infrared photography for determining early in-season nitrogen requirements in corn. Agron. J. 98 (4), 968–977. https://doi.org/10.2134/agronj2005.0200.
Tataridas, A., Jabran, K., Kanatas, P., Oliveira, R.S., Freitas, H., Travlos, I., 2022. Early detection, herbicide resistance screening, and integrated management of Invasive Plant Species: a review. Pest Manag. Sci. 78 (10), 3957–3972. https://doi.org/10.1002/ps.6963.
Theron, K.J., Pryke, J.S., Latte, N., Samways, M.J., 2022. Mapping an alien invasive shrub within conservation corridors using super-resolution satellite imagery. J. Environ. Manag. 321, 116023 https://doi.org/10.1016/j.jenvman.2022.116023.
Ullah, S., Si, Y., Schlerf, M., Skidmore, A.K., Shafique, M., Iqbal, I.A., 2012. Estimation of grassland biomass and nitrogen using MERIS data. Int. J. Appl. Earth Obs. Geoinf. 19, 196–204. https://doi.org/10.1016/j.jag.2012.05.008.
Villalobos Perna, P., Di Febbraro, M., Carranza, M.L., Marzialetti, F., Innangi, M., 2023. Remote sensing and invasive plants in coastal ecosystems: what we know so far and future prospects. Land 12 (2), 341. https://doi.org/10.3390/land12020341.
Villoslada, M., Bergamo, T.F., Ward, R.D., Burnside, N.G., Joyce, C.B., Bunce, R.G.H., Sepp, K., 2020. Fine scale plant community assessment in coastal meadows using UAV based multispectral data. Ecol. Indicat. 111, 105979 https://doi.org/10.1016/j.ecolind.2019.105979.
Villoslada, M., Bergamo, T.F., Ward, R.D., Joyce, C.B., Sepp, K., 2021. A novel UAV-based approach for biomass prediction and grassland structure assessment in coastal meadows. Ecol. Indicat. 122, 107227 https://doi.org/10.1016/j.ecolind.2020.107227.
Villoslada, M., Sipelgas, L., Bergamo, T.F., Ward, R.D., Reintam, E., Astover, A., et al., 2022. Multi-source remote sensing data reveals complex topsoil organic carbon dynamics in coastal wetlands. Ecol. Indicat. 143, 109329 https://doi.org/10.1016/j.ecolind.2022.109329.
Wan, H., Wang, Q., Jiang, D., Fu, J., Yang, Y., Liu, X., 2014. Monitoring the invasion of Spartina alterniflora using very high resolution unmanned aerial vehicle imagery in beihai, guangxi (China). Sci. World J., 638296 https://doi.org/10.1155/2014/638296, 2014.
Wang, R., Gamon, J.A., Cavender-Bares, J., Townsend, P.A., Zygielbaum, A.I., 2018. The spatial sensitivity of the spectral diversity–biodiversity relationship: an experimental test in a prairie grassland. Ecol. Appl. 28 (2), 541–556. https://doi.org/10.1002/eap.1669.
Ward, R.D., Burnside, N.G., Joyce, C.B., Sepp, K., 2016. Importance of microtopography in determining plant community distribution in Baltic Coastal Wetlands. J. Coast Res. 32 (5), 1062–1070. https://doi.org/10.2112/JCOASTRES-D-15-00065.1.
Ward, R., Burnside, N., Joyce, C., Sepp, K., 2013. The use of medium point density LiDAR elevation data to determine plant community types in Baltic coastal wetlands. Ecol. Indicat. 33, 96–104.
Ward, R., Burnside, N., Joyce, C., Sepp, K., Teasdale, P.A., 2014. Recent rates of sedimentation on irregularly flooded Boreal Baltic coastal wetlands: responses to recent changes in sea level. Geomorphology 217, 61–72.
Weidlich, E.W., Flórido, F.G., Sorrini, T.B., Brancalion, P.H., 2020. Controlling invasive plant species in ecological restoration: a global review. J. Appl. Ecol. 57 (9), 1806–1817. https://doi.org/10.1111/1365-2664.13656.
Westoby, M.J., Brasington, J., Glasser, N.F., Hambrey, M.J., Reynolds, J.M., 2012. 'Structure-from-Motion'photogrammetry: a low-cost, effective tool for geoscience applications. Geomorphology 179, 300–314. https://doi.org/10.1016/j.geomorph.2012.08.021.
Wu, S., Wang, J., Yan, Z., Song, G., Chen, Y., Ma, Q., et al., 2021. Monitoring tree-crown scale autumn leaf phenology in a temperate forest with an integration of PlanetScope and drone remote sensing observations. ISPRS J. Photogrammetry Remote Sens. 171, 36–48. https://doi.org/10.1016/j.isprsjprs.2020.10.017.
Yan, Y., 2016. MLmetrics: Machine Learning Evaluation Metrics. Available online: https://cran.r-project.org/web/packages/MLmetrics/. (Accessed 8 February 2023).
Yang, W., Wang, S., Zhao, X., Zhang, J., Feng, J., 2015. Greenness identification based on HSV decision tree. Information Processing in Agriculture 2 (3–4), 149–160. https://doi.org/10.1016/j.inpa.2015.07.003.
Yang, Y., Wu, T., Wang, S., Li, H., 2020. Fractional evergreen forest cover mapping by MODIS time-series FEVC-CV methods at sub-pixel scales. ISPRS J. Photogrammetry Remote Sens. 163, 272–283. https://doi.org/10.1016/j.isprsjprs.2020.03.012.
Yemshanov, D., Haight, R.G., MacQuarrie, C.J., Simpson, M., Koch, F.H., Ryan, K., Bullas-Appleton, E., 2022. Hierarchical governance in invasive species survey campaigns. Ecol. Econ. 201, 107551 https://doi.org/10.1016/j.ecolecon.2022.107551.
Zhang, H., Eziz, A., Xiao, J., Tao, S., Wang, S., Tang, Z., et al., 2019. High-resolution vegetation mapping using eXtreme gradient boosting based on extensive features. Rem. Sens. 11 (12), 1505. https://doi.org/10.3390/rs11121505.
Zhang, S., Isermann, M., Gan, W., Breed, M., 2018. Invasive Rosa rugosa populations outperform native populations, but some populations have greater invasive potential than others. Sci. Rep. 8 (1), 1–8. https://doi.org/10.1038/s41598-018-23974-3.
Zhao, J., Zhou, C., Huang, L., Yang, X., Xu, B., Liang, D., 2018. Fusion of unmanned aerial vehicle panchromatic and hyperspectral images combining joint skewness-kurtosis figures and a non-subsampled contourlet transform. Sensors 18 (10), 1–23. https://doi.org/10.3390/s18103467.
Zhong, L., Hu, L., Zhou, H., 2019. Deep learning based multi-temporal crop classification. Rem. Sens. Environ. 221, 430–443. https://doi.org/10.1016/j.rse.2018.11.032.
Zvoleff, A., 2020. Package 'glcm'. Calculate Textures from Grey-Level Co-occurence Matrices (GLCMs). Available online: https://CRAN. R-project. org/package= glcm. (Accessed 19 August 2021).